VOL. 21, NO. 6, MARCH 2026 ISSN 1819-6608
ARPN Journal of Engineering and Applied Sciences

www.arpnjournals.com

DYNAMIC RHEOLOGICAL AND STRUCTURAL CHARACTERIZATION OF REVERSIBLY CROSSLINKED HDPE COMPOSITES REINFORCED WITH POLYETHYLENE TEREPHTHALATE FIBERS AND GRAPHENE

R. Nemri[1,2], S. Bouhelal[1,2], E. Roumeli[3], K. Chrissafis[3] and D. Bikiaris[4]
[1]Laboratoire des Matériaux Polymériques Multiphasiques (LMPMP), Faculty of Engineering, Ferhat Abbas University of Setif-1, Sétif, Algeria
[2]Unite de Recherche des Matériaux Emergents de Setif (URMES), Ferhat Abbas University of Setif-1, Sétif, Algeria
[3]Solid State Physics Department, School of Physics, Aristotle University of Thessaloniki, Thessaloniki, Greece
[4]Laboratory of Polymer Chemistry and Technology, Department of Chemistry, Aristotle University of Thessaloniki, Thessaloniki, Greece
E-Mail: nemripoly@univ-setif.dz

ABSTRACT

This study investigates the potential of reversible crosslinking reaction (RXR) as a matrix modification strategy for high-density polyethylene (HDPE) to combine network-like performance with recyclability. Dynamic rheological analysis revealed pronounced increases in melt viscosity and development of solid-like responses, confirming dynamic network formation. Incorporation of polyethylene terephthalate (PET) fibers at 3, 7, and 10 wt% enhanced crystallinity from 68.5% (neat HDPE) to 74.9% (7 wt% fiber), demonstrating the strong nucleating effect of fibers. Further enhancement to 80.2% crystallinity was achieved through the addition of 5 wt% maleic anhydride grafted polyethylene (MAH) compatibilizer, which significantly improved fiber-matrix interfacial adhesion. Incorporation of graphene at 0.5, 1, and 3 wt% provided additional nucleation sites, achieving crystallinity of 78.6% at 3 wt% graphene with refined crystallite sizes. Scanning electron microscopy revealed a pronounced transformation from clean fiber pull-out in non-compatibilized systems to extensive fiber fracture with matrix residue in MAH-compatibilized composites, confirming superior interfacial bonding. Thermogravimetric analysis demonstrated thermal stabilization with decomposition temperatures shifted by up to 15 °C in graphene-reinforced systems compared to neat HDPE. The strategic combination of dynamic crosslinking with multi-scale reinforcement produces hybrid composites with significantly enhanced crystallinity, refined microstructure, improved thermal stability, superior interfacial quality, and retained thermal recyclability, offering promising applications in sustainable, high-performance polymer composites.

Keywords: reversible crosslinking reaction (RXR), high-density polyethylene (HDPE), Polyethylene terephthalate (PET) fibers, polymer composites, dynamic rheological analysis.

Manuscript Received 3 May 2026; Revised 25 March 2026; Published 20 May 2026

1. INTRODUCTION

High-density polyethylene (HDPE) is one of the most widely used thermoplastic polymers in industrial applications owing to its attractive balance of mechanical strength, chemical resistance, low density, and ease of processing. Nevertheless, for many advanced structural applications and long-term service conditions, there is continuous demand for materials exhibiting higher stiffness, better thermal resistance, superior creep performance, and extended operational lifetime, while ideally maintaining the ability to be recycled at the end of service life. Conventional crosslinking strategies, typically employing peroxide-based chemistry, can effectively improve the dimensional stability and resistance of HDPE, but they rely on permanent covalent bonds that irreversibly lock the polymer network and drastically compromise melt reprocessability and recyclability [1].

Reversible crosslinking reactions (RXR) have emerged in recent years as an innovative approach to overcome these inherent limitations by introducing dynamic covalent bonds between polymer chains [2]. These reversible bonds can be dissociated and reformed under appropriate thermal conditions, allowing the material to behave like a crosslinked network in solid and melt states while retaining the capacity to be reshaped, reprocessed, and recycled when needed. Previous investigations on RXR-modified HDPE have reported pronounced changes in rheological behavior, including increased melt viscosity and solid-like mechanical responses, alongside modifications in crystalline structure and phase composition, as confirmed by dynamic rheological analysis, differential scanning calorimetry, and X-ray diffraction studies [3]. Such materials bridge the gap between classic thermoplastics and thermosets in terms of performance characteristics and processability.

In the first part of the present work, two RXR routes were applied to HDPE to establish a reversible dynamic network and to investigate the effects of this network on the melt rheology and semicrystalline morphology of the base matrix systematically. The evolution of torque and melt viscosity during the reaction was followed by dynamic rheological analysis (DRA), providing direct evidence of network build-up and the development of increasingly elastic melt responses. The

impact of RXR on crystallinity and crystallite size was assessed using differential scanning calorimetry (DSC) and wide-angle X-ray scattering (WAXS), while thermogravimetric analysis (TGA/DTG) evaluated the thermal stability of the newly formed dynamic network.

Polymer composites reinforced with fibers have become key materials in applications where low weight must be combined with high stiffness and strength. Polyethylene terephthalate (PET) fibers, in particular, offer high modulus, good thermal stability, and relatively low cost, making them attractive candidates for reinforcing HDPE-based systems. Numerous studies have demonstrated that PET fiber incorporation into polyolefin matrices can significantly improve stiffness, creep resistance, and dimensional stability at elevated temperatures [4, 5]. However, differences in polarity, chemical structure, and surface energy between the hydrophobic HDPE and the polar PET polymer frequently result in poor interfacial adhesion, fiber pull-out, and inefficient stress transfer across the matrix–fiber boundary, severely limiting the achievable mechanical improvements.

To address interfacial incompatibility and adhesion challenges, various compatibilization strategies have been developed, including fiber surface modifications and the introduction of functionalized polyolefins. Maleic anhydride grafted polyethylene (MAH) has proven to be an effective compatibilizer, since the anhydride groups can establish covalent or hydrogen-bonded interactions with hydroxyl and carboxyl groups on the PET fiber surface, promoting stronger interfacial bonding [6]. Beyond conventional compatibilization, the presence of a reversible crosslinked network in the HDPE matrix offers an additional mechanism for enhancing stress transfer and structural integrity, while simultaneously preserving the possibility of thermal reshaping and recycling. Furthermore, the introduction of nanoscale fillers such as graphene provides yet another level of reinforcement through nano-scale nucleation effects and barrier properties, potentially enhancing stiffness, thermal stability, and long-term performance when adequate dispersion is achieved.

In the second part of this study, polyethylene terephthalate fibers were incorporated into the reversibly crosslinked HDPE matrix at varying loadings (3, 7, and 10 wt%), and selected formulations were further modified with 5 wt% MAH compatibilizer and varying graphene content (0.5, 1, and 3 wt%). This multi-component composite architecture aims to combine the advantages of a dynamic network, micro-scale fiber reinforcement, and nano-scale graphene reinforcement into a single optimized system. The influence of PET fibers, MAH compatibilizer, and graphene on crystallization behavior, crystallinity, crystallite morphology, and thermal stability was systematically investigated using DSC, WAXS, and TGA/DTG. Morphological observations by scanning electron microscopy (SEM) were conducted to assess fiber dispersion, interfacial adhesion quality, and graphene distribution in the various composite formulations.

The overall objective of this investigation is twofold: first, to elucidate the effects of RXR on the rheological and structural properties of HDPE; and second, to demonstrate how PET fibers, chemical compatibilization, and graphene can be synergistically combined with a reversibly crosslinked matrix to produce hybrid HDPE-based composites with significantly enhanced stiffness, improved thermal behavior, refined microstructure, and retained recyclability. By integrating dynamic covalent chemistry with micro- and nano-reinforcement strategies, the proposed materials represent a promising class of sustainable, high-performance polymer composites suitable for modern engineering applications.

2. EXPERIMENTAL

2.1 Materials

High-density polyethylene (HDPE, HYA 600, ExxonMobil Chemical, USA; $\rho = 0.954$ g/cm³, MFI = 0.37 g/10 min at 190 °C/2.16 kg) was used as the matrix. The reversible crosslinking system comprised di(tert-butylperoxyisopropyl)benzene (DTBPIB, Perkadox 14-40 B-gr, Akzo Nobel, Netherlands) as peroxide initiator, tetramethylthiuram disulfide (TMTDS, Rhodia, France) as accelerator, and elemental sulfur (S_8, Wuxi Huasheng, China) as dynamic crosslinking agent.

Hollow recycled poly(ethylene terephthalate) (rPET) fibers were supplied by TINER-PLAST (Sétif, Algeria) from post-consumer carbonated drink bottles (ρ = 1.32 g/cm³, elongation at break = 55%, Tm = 250 °C). Maleic anhydride (Sigma-Aldrich, USA, 99% purity) served as a compatibilizer. Few-layer graphene powder (Sigma-Aldrich, product 900561, USA; $\sigma > 10^3$ S/m, <3 layers, lateral size 0.5-5 μm, SSA >500 m²/g) was incorporated as a nanofiller.

2.2 Processing

The fabrication of the composites was carried out in two consecutive steps. First, the reversible crosslinking (RXR) of the HDPE matrix was performed. The base RXR formulation, designated as PEX, was prepared by mixing 100 phr of HDPE with 0.8 phr of peroxide, 0.4 phr of sulfur, and 0.2 phr of TMTDS. The compounding was conducted in an internal mixer (Brabender Plastograph, Germany) at 170 °C and 30 rpm for 30 minutes, allowing for real-time monitoring of the torque evolution.

In the second step, the pre-crosslinked RXR-HDPE (PEX) was ground into granules and subsequently melt-mixed with varying proportions of PET fibers, MAH, and graphene powder to produce the final composites. The mixing was also performed in the Brabender Plastograph under the same temperature and rotor speed conditions for 15 minutes to ensure homogeneous dispersion.

The specific composition and coding of all prepared materials are detailed in Table-1.

Table-1. Samples composition.

Sample Group	Sample Code	RXR-HDPE (PEX) (phr)	rPET Fibers (phr)	MAH (phr)	Graphene Powder (phr)
Reference	PE0	-	-	-	-
RXR Matrix	PEX	100	-	-	-
With Fibers	PEX3F	100	3	-	-
	PEX7F	100	7	-	-
	PEX10F	100	10	-	-
With Fibers & MAH	PEX3F-5MAH	100	3	5	-
	PEX7F-5MAH	100	7	5	-
	PEX10F-5MAH	100	10	5	-
With Fibers and Graphene Powder	PEX3F-0.5gr	100	3	-	0.5
	PEX3F-1gr	100	3	-	1
	PEX3F-3gr	100	3	-	3

The compounded materials were then ground and processed into test specimens via compression molding using a Paul-Otto Weber press (Germany) at 190 °C under a pressure of 30 kN for 3 minutes, followed by cooling under pressure.

2.3 Characterization Techniques

2.3.1 Dynamic Rheological Analysis (DRA)

was performed directly during the mixing process in the Brabender Plastograph. Torque-time curves were recorded for each formulation to monitor the crosslinking and compounding behavior in the melt state.

2.3.2 Thermal properties

were analyzed using a Setaram DSC-141 differential scanning calorimeter. Samples of approximately 5 mg were sealed in aluminum pans. The thermal program involved heating from 20 °C to 180 °C at 10 °C/min, holding for 5 minutes to erase thermal history, cooling to 40 °C at 5 °C/min, and a second heating scan to 180 °C at 10 °C/min. The degree of crystallinity (χc) was calculated using Equation (1):

$$X_c = \frac{\Delta H_m}{(1-\emptyset)\Delta H_m^0} \times 100 \ldots\ldots\ldots \text{Eq.} \quad (1)$$

where ΔHm is the measured melting enthalpy from the second heating scan, ϕ is the weight fraction of the non-crystalline filler, and ΔH_m^0 is the melting enthalpy of 100% crystalline HDPE (293 J/g) [7].

2.3.3 Thermogravimetric analysis (TGA)

was performed on a Setaram Labsys Evo instrument. Samples of about 7 mg were heated from 30 °C to 700 °C at a rate of 20 °C/min under a nitrogen atmosphere to assess thermal stability.

2.3.4 Wide-Angle X-ray Scattering (WAXS)

Measurements were conducted using a Bruker D8 Advance X-ray diffractometer with Cu Kα radiation (λ = 1.54 Å). The scans were recorded in the 2θ range of 5° to 50°. The crystallite size (Lc) was calculated from the (110) reflection peak using the Debye-Scherrer equation (Equation 2):

$$L_C = \frac{k.\lambda}{\beta.\cos\theta} \ldots\ldots\ldots \text{Eq.} \quad (2)$$

where k is the shape factor (0.9), λ is the X-ray wavelength, β is the full width at half maximum (FWHM) of the diffraction peak in radians, and θ is the Bragg angle.

2.3.5 Scanning Electron Microscopy (SEM)

was used to examine the morphology of the fracture surfaces and the dispersion of fibers and graphene. The fracture surfaces of impact-test specimens were sputter-coated with a thin layer of gold and imaged using a JEOL JSM-6390 LV microscope.

3. RESULTS AND DISCUSSIONS

3.1 Rheological Properties of the RXR Matrix

The rheological behavior of HDPE during the reversible crosslinking reaction (RXR) was monitored in situ by dynamic rheological analysis (DRA) using a Haake torque rheometer at 180 °C under a nitrogen atmosphere. Figure-1(a) presents the evolution of torque as a function of mixing time for neat HDPE (PE0) and the reversibly crosslinked sample (PEX). Neat HDPE shows stable torque post-melting, characteristic of a linear thermoplastic melt with no significant structural changes during mixing. In contrast, the PEX sample shows a pronounced and continuous increase in torque throughout the reaction period, reaching values substantially higher than those of PE0. This systematic rise in torque is a direct

manifestation of the progressive formation of a three-dimensional network structure within the melt, as reversible sulfur-based linkages are established between polyethylene chains [3, 8].

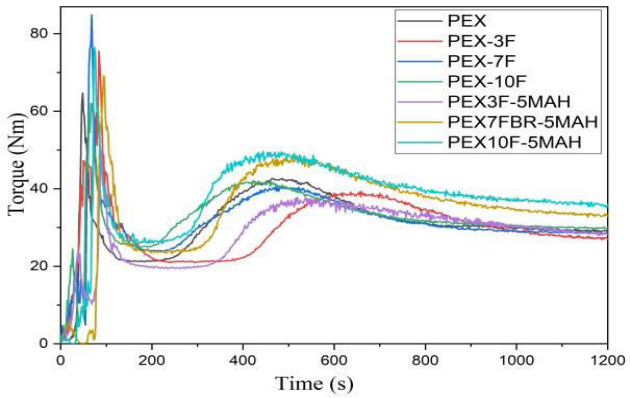

(a)

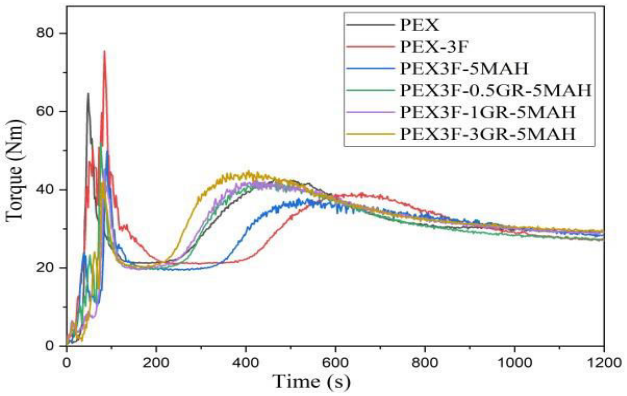

(b)

Figure-1. Dynamic Rheological Analysis: (a) for PEX and all PEXs with PET fibers; (b) for PEX and PEXs with 3% PET fibers and graphene powder.

The increase in torque reflects a corresponding increase in melt viscosity, which indicates that the flowability of the polymer is being progressively restricted by the growing network. This behavior is fully consistent with the formation of a dynamic crosslinked architecture, where chain mobility is constrained by reversible interchain bonds, leading to a more elastic and less fluid-like response. The continuous nature of the torque increase suggests that the crosslinking reaction proceeds steadily over the entire mixing time, without reaching a plateau within the experimental timeframe, implying that further network development could potentially be achieved with extended reaction times or optimized formulations [9].

This reduction in flowability is a key characteristic of reversibly crosslinked systems, where the melt behaves more like a viscoelastic gel than a simple viscous liquid [10]. Importantly, the sulfur-based crosslinks responsible for this behavior are thermally reversible [11], meaning that they can dissociate at elevated temperatures and reform upon cooling, thereby enabling repeated melt processing and recycling-a feature that distinguishes RXR systems from conventional peroxide-crosslinked networks. The rheological data thus demonstrate that the HDPE matrix has been successfully modified to combine the processing advantages of thermoplastics with the dimensional stability and mechanical performance typically associated with thermosets.

When PET fibers were subsequently incorporated into the reversibly crosslinked matrix at varying loadings, further changes in rheological behavior were observed, as illustrated in Figure-1 (b). The addition of 3 wt% PET fibers without compatibilizer (sample PEX3F) leads to a noticeable increase in torque compared to the fiber-free PEX matrix, reflecting the additional resistance to flow imposed by the rigid fiber network dispersed in the melt. This torque increase is consistent with the well-known reinforcing effect of fibers in polymer composites, where the presence of a percolating fiber structure restricts polymer chain movement and increases the effective viscosity of the composite melt. Further torque increases are observed at 7 wt% (PEX7F) and 10 wt% (PEX10F) fiber loadings [12], indicating a loading-dependent enhancement in melt viscosity.

When 5 wt% maleic anhydride grafted polyethylene (MAH) compatibilizer is introduced alongside the PET fibers-samples designated as PEX3F-5MAH, PEX7F-5MAH, and PEX10F-5MAH-a further substantial increase in torque is consistently observed across all fiber loadings, reaching significantly higher values than the non-compatibilized composites. This additional torque rise can be attributed to improved fiber-matrix adhesion facilitated by the MAH compatibilizer, which promotes chemical or physical bonding between the polar PET fiber surface and the HDPE matrix. Enhanced interfacial adhesion results in more effective stress transfer from the matrix to the fibers, increasing the resistance to deformation and leading to a higher overall melt viscosity. At the same time, the improved wetting and dispersion of fibers in the compatibilized system may also contribute to the observed rheological response.

The incorporation of graphene at 0.5 wt%, 1 wt%, and 3 wt% (samples PEX3F-0.5gr, PEX3F-1gr, and PEX3F-3gr, respectively) into the base fiber formulation results in progressive further increases in torque. Graphene, when well dispersed, can form a percolating network at very low loadings due to its high aspect ratio and large surface area; thereby further restricting polymer chain mobility and increasing melt viscosity. The torque values increase systematically with graphene content, with the highest levels recorded at 3 wt% graphene addition (sample PEX3F-3gr), confirming that the combined effect of reversible crosslinking, PET fiber reinforcement at 3 wt%, compatibilization with MAH, and progressive graphene incorporation produces synergistic enhancements in composite melt viscosity and structural stability.

Overall, the rheological results provide clear and systematic evidence that the RXR process successfully modifies the HDPE matrix into a dynamic network, and that subsequent incorporation of PET fibers at different loadings, MAH compatibilizer, and graphene produces progressive and synergistic effects on melt viscosity and structural stability. These rheological changes are expected to translate into improved mechanical properties, better dimensional stability at elevated temperatures, and enhanced resistance to creep and deformation under load, while the reversible nature of the crosslinks ensures that the composites retain the ability to be reprocessed and recycled [13].

3.2 Structural Properties and Crystallization Behavior DSC and WAXS Analysis

The influence of the reversible crosslinking reaction (RXR) and the subsequent reinforcement with PET fibers and graphene on the crystalline microstructure [7] of HDPE was comprehensively investigated using differential scanning calorimetry (DSC) (Figure-2) and wide-angle X-ray scattering (WAXS) (Figure-3). The thermal and structural properties obtained from these analyses are summarized in Table-2, which includes the melting temperature (Tm), crystallization temperature (Tc), melting enthalpy (ΔHm), degree of crystallinity (χc), and crystallite thickness (Lc).

The neat HDPE reference sample (PE0) exhibits a crystallinity of 68.5% with an average crystallite thickness of 24.5 nm, characteristic of the semicrystalline nature of linear polyethylene. The RXR-modified HDPE matrix (PEX), produced through the reversible crosslinking process, shows a marginal decrease in crystallinity to 68.3%, a subtle but notable effect attributable to the constraints imposed by the newly formed dynamic network on chain mobility and polymer chain rearrangement during crystallization. The crosslinked network restricts the cooperative segmental motion necessary for optimal crystal nucleation and growth, resulting in a slight reduction in the overall crystalline fraction. However, the crystallite size (Lc = 22.2 nm) remains comparable to PE0, indicating that the crosslinking does not grossly disrupt the crystalline lattice structure.

Table-2. Thermal and structural properties from DSC and WAXS.

Sample	Tm (°C)	Tc (°C)	ΔHm (J/g)	χc (%)	Lc (nm)
PE0	133.3	114.3	138.7	68.5	24.5
PEX	131.2	115.9	138.3	68.3	22.2
PEX3F	130.6	115.5	139.7	71.1	21.4
PEX7F	130.3	115.5	141.0	74.9	21.0
PEX10F	130.6	115.1	136.2	74.7	22.0
PEX3F-5MAH	133.0	112.7	136.3	73.2	24.5
PEX7F-5MAH	130.8	115.6	143.0	80.2	21.1
PEX10F-5MAH	130.1	115.4	129.4	75.2	22.6
PEX3F-0.5gr	132.2	113.2	144.1	77.8	22.4
PEX3F-1gr	130.6	114.6	143.8	78.0	20.8
PEX3F-3gr	129.9	115.3	141.6	78.6	20.5

A dramatic reversal of this trend occurs upon incorporation of PET fibers into the RXR matrix. The PET fibers function as highly effective nucleating agents, promoting heterogeneous nucleation and leading to a pronounced increase in crystallinity. Sample PEX3F (containing 3 wt% PET fibers) shows an increase in crystallinity to 71.1%, while sample PEX7F (7 wt% PET fibers) reaches 74.9%, demonstrating a clear loading-dependent enhancement. The crystallite size simultaneously decreases from 24.5 nm (PE0) to 21.4 nm (PEX3F) and further to 21.0 nm (PEX7F), indicating a finer and more refined crystalline morphology. This reduction in crystallite thickness is a direct consequence of the increased number of nucleation sites provided by the well-dispersed PET fibers, which promote the formation of a larger population of smaller crystallites rather than a few large spherulites. Such fine-grained microstructures are highly advantageous from a mechanical perspective, as they enhance crack deflection and energy absorption capabilities.

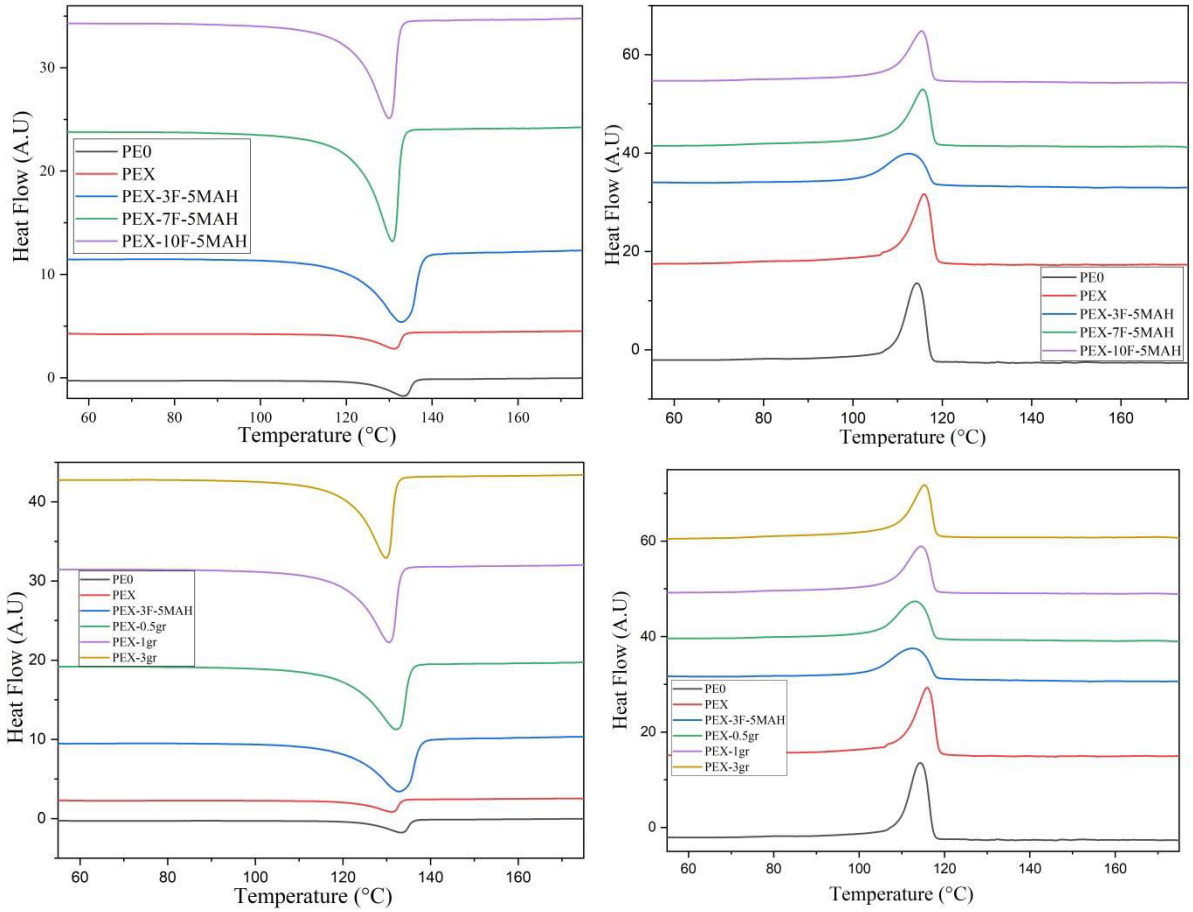

Figure-2. Heating/cooling diagrams: (a) Heating curves for PEX and all PEXs with PET fibers; (b) Cooling curves for PEX and all PEXs with PET fibers; (c) Heating curves for PEX and PEX with 3% PET fibers and graphene; (d) Cooling curves for PEX and PEX with 3% PET fibers and graphene.

Most significantly, the addition of 5 wt% maleic anhydride grafted polyethylene (MAH) compatibilizer induces a synergistic enhancement of the crystallization behavior. Sample PEX7F-5MAH achieves the highest crystallinity recorded in this study, reaching 80.2%-an increase relative to both the neat HDPE (PE0) and the non-compatibilized fiber-reinforced composites. The crystallinity achieved (80.2%) surpasses commonly reported values for HDPE composites (≈70-75%) [7, 14], highlighting the synergistic effect of fiber-induced nucleation and enhanced interfacial compatibility introduced by MAH. This superior nucleation efficiency is attributed to the dual-functional role of MAH in the composite system. The maleic anhydride groups on the PE backbone react chemically with hydroxyl and carboxyl end groups present on the PET fiber surface, establishing covalent linkages that effectively anchor the polymer chains to the fiber surface. Simultaneously, the hydrocarbon backbone of MAH entangles and interpenetrates with the HDPE matrix chains, creating a continuous and highly efficient interface. This engineered interfacial architecture transforms every point on the fiber surface into a highly active nucleation site, amplifying the heterogeneous nucleation efficiency.

Concurrently with the crystallinity increase, the MAH-compatibilized samples show further refinement in crystallite size. Sample PEX7F-5MAH exhibits a crystallite thickness of 21.1 nm, among the smallest values observed across the study, confirming that the improved interfacial bonding not only increases the total crystalline fraction but also promotes the formation of a denser population of finer crystallites. This crystalline architecture - high crystallinity combined with small crystallite size - represents the optimal morphology for delivering superior mechanical stiffness and toughness.

The melting temperature (Tm) and crystallization temperature (Tc) remain largely invariant across all sample series, fluctuating only slightly within a narrow range of 129.9-133.3 °C and 112.7-115.9 °C, respectively (Table-2). This stability demonstrates that the reinforcements and compatibilizers do not fundamentally alter the thermodynamic stability or the melting behavior of the HDPE crystalline lattice; rather, they selectively modulate the kinetics of crystallization and the density of nucleation events.

The incorporation of graphene into the 3 wt% PET fiber composites further enhances the crystalline properties through additional nano-scale nucleation effects. Sample PEX3F-0.5gr (0.5 wt% graphene) exhibits a crystallinity of 77.8%, while samples PEX3F-1gr (1 wt% graphene) and PEX3F-3gr (3 wt% graphene) achieve crystallinities of 78.0% and 78.6%, respectively [15]. The graphene, with its extremely high aspect ratio and large surface area, acts as an exceptional nano-scale nucleating agent even at very low loadings [16]. The continuous increase in crystallinity from 0.5 wt% to 3 wt% graphene indicates a systematic nucleation effect that does not saturate within the tested concentration range. Correspondingly, the crystallite sizes for these graphene-containing samples are among the finest recorded in the entire study, with values of 22.4 nm, 20.8 nm, and 20.5 nm for 0.5, 1, and 3 wt% graphene, respectively. The sample containing 3 wt% graphene (PEX3F-3gr) achieves the smallest crystallite thickness at 20.5 nm, indicating that the combination of fiber and graphene reinforcement creates the most densely nucleated system.

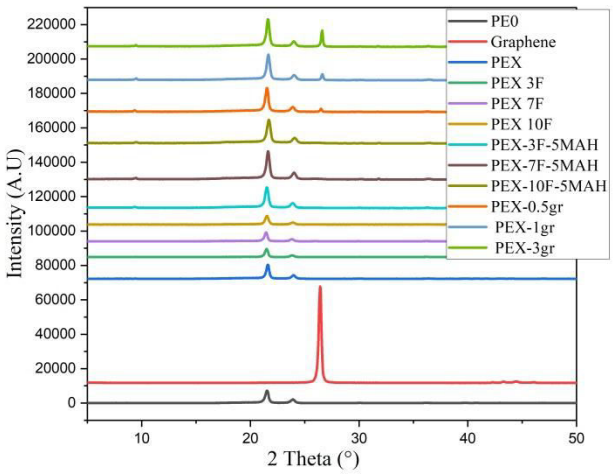

Figure-3. WAXS curves for PE0, PEX, and graphene with all modified PEXs.

Overall, the DSC and WAXS results reveal a clear and systematic hierarchy of crystallization behavior driven by the strategic introduction of reinforcements and compatibilization. The progression from neat HDPE to the reversibly crosslinked matrix, fiber-reinforced composites, MAH-compatibilized systems, and finally graphene-containing hybrids demonstrates cumulative and synergistic effects on both the degree of crystallinity and the refinement of the crystalline morphology. These structural enhancements, supported by the rheological and morphological analyses, may contribute to improved mechanical performance, dimensional stability, creep resistance, and the overall structural integrity of the resulting composite materials.

3.3 Morphological Analysis (SEM)

Scanning Electron Microscopy (SEM) was employed to visualize the fracture morphology of the composites and assess the dispersion of reinforcements within the matrix, as well as to evaluate the quality of interfacial adhesion between the fibers and the surrounding polymer matrix. Representative micrographs documenting the morphological features of all composite series are presented in Figure-4.

A. Fiber-Reinforced Composites without Compatibilizer (PEX3F, PEX7F, PEX10F)

The SEM micrographs of the non-compatibilized fiber composites, exemplified by samples PEX3F and PEX7F (Figure-4 (a)), reveal pronounced signs of poor interfacial adhesion between the PET fibers and the HDPE matrix. The PET fibers exhibit clean and smooth surfaces where they have been extracted from the matrix during fracture, leaving behind characteristic void spaces and fiber-shaped cavities in the polymer. This clean fiber pull-out phenomenon is a classic morphological signature of weak fiber-matrix bonding, where interfacial shear strength is insufficient to transfer stress from the matrix to the reinforcement phase [17]. Such inadequate adhesion severely compromises the load-bearing capability of the reinforcement and leads to inefficient stress transfer, ultimately limiting the achievable mechanical performance despite the presence of high-modulus PET fibers.

The gaps and separations visible between the fiber surface and the surrounding matrix are direct visual evidence of debonding and lack of chemical or physical interaction at the interface. These voids are expected to act as stress concentration sites, initiating crack propagation and premature failure under mechanical loading. From a fracture mechanics perspective, the low interfacial adhesion allows the fibers to decouple from the load-bearing matrix, negating the reinforcement benefit that the fibers might otherwise provide.

B. Fiber-Reinforced Composites with MAH Compatibilizer (PEX3F-5MAH, PEX7F-5MAH, PEX10F-5MAH)

A striking transformation in morphology occurs upon the incorporation of the MAH compatibilizer. The SEM images of the MAH-containing composites (Figure-4 (b)) present a starkly different appearance compared to the non-compatibilized samples. Rather than the clean pull-out observed in PEX3F and PEX7F, the fibers in MAH-compatibilized samples such as PEX3F-5MAH and PEX7F-5MAH are frequently fractured rather than pulled out, indicating that the fibers now possess sufficient bond strength with the surrounding matrix to resist extraction during fracture.

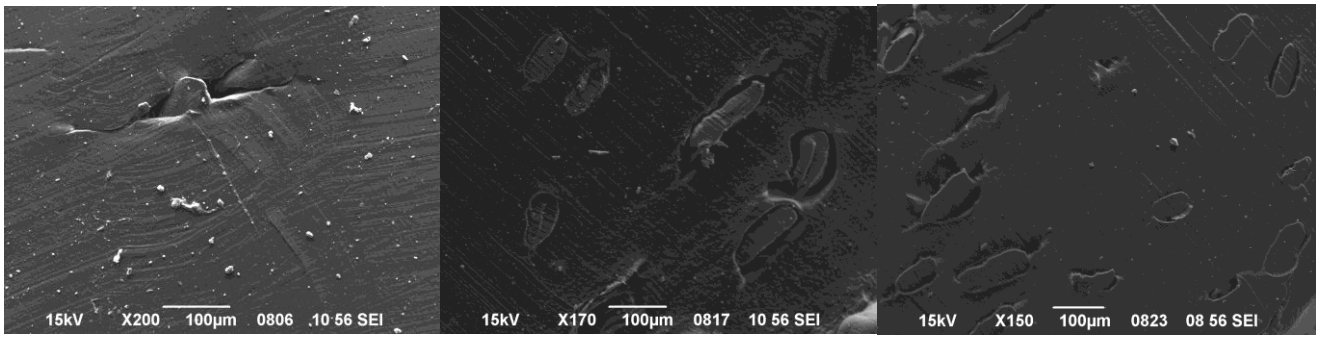

a) PEX3F: PEX7F: PEX10F:

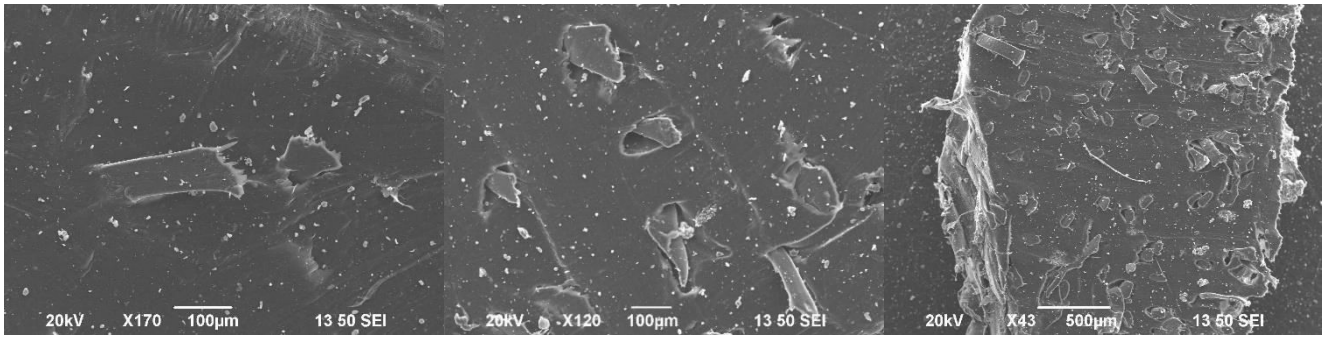

b) PEX3F-5MAH: PEX7F-5MAH: PEX10F-5MAH:

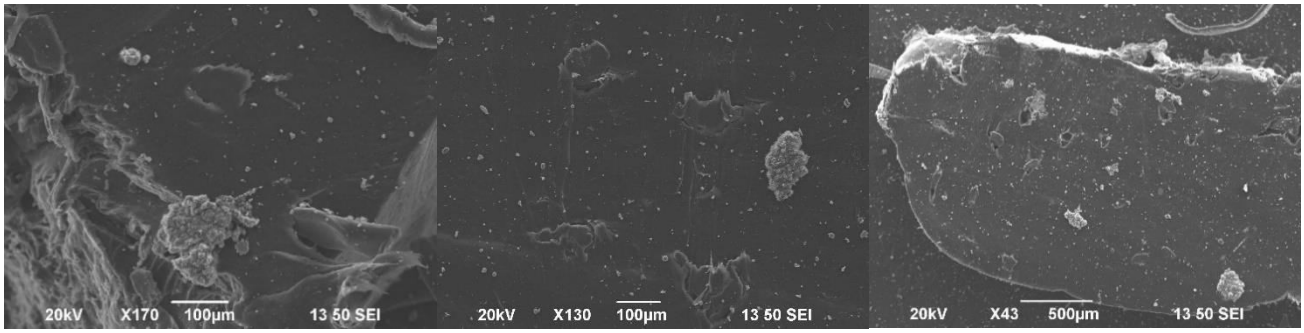

c) Graphene: 0,5% Graphene: 1% Graphene: 3%

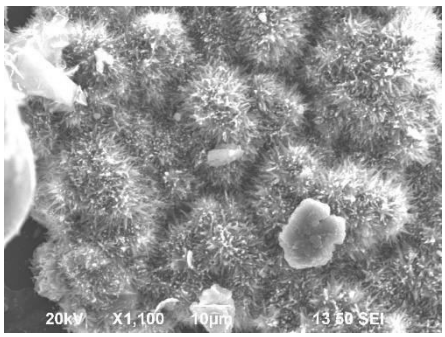

d) Graphene particle

Figure-4. SEM: (a) microscopy for PEXs with PET fibers; (b) microscopy for PEXs with PET fibers and MAH; (c) microscopy for PEXs with 3% PET fibers and graphene; (d) microscopy for graphene powder.

Critically, the fractured fiber ends are surrounded by rough and textured matrix residue that remains tightly adhered to the fiber surface, indicating strong interfacial bonding and matrix attachment. No visible gaps or voids are present between the fiber and matrix in these samples, demonstrating that the MAH compatibilizer has successfully engineered a continuous and robust interface. This adhesive layer represents both physical

interpenetration of the HDPE matrix with the PE backbone of the MAH and chemical interaction between the maleic anhydride groups and the polar PET fiber surface.

The transition from fiber pull-out to fiber fracture, combined with the absence of interfacial voids, provides direct and unambiguous morphological evidence that the MAH compatibilizer significantly elevates the interfacial shear strength [18]. This enhanced adhesion enables efficient stress transfer from the matrix to the fiber, such that both phases participate actively in carrying the applied load. The improved load transfer capability, when combined with the elevated crystallinity (80.2% for PEX7F-5MAH, as shown in Table II) and refined crystallite structure, results in the composite exhibiting superior stiffness, strength, and impact resistance.

C. Graphene-Reinforced Composites (PEX3F-0.5gr, PEX3F-1gr, PEX3F-3gr)

The SEM micrographs of the graphene-reinforced composites at higher magnification (Figure-4 (c)) reveal that the graphene is generally well-dispersed throughout the HDPE matrix with only minimal agglomeration. At the lowest loading of 0.5 wt% graphene (PEX3F-0.5gr), the nanoplatelets are uniformly distributed within the matrix with no visible clusters or bundles. At the intermediate loading of 1 wt% graphene (PEX3F-1gr), the dispersion remains homogeneous with only occasional minor agglomerations visible (Figure-4 (d)).

Even at the highest graphene loading of 3 wt% (PEX3F-3gr), the nanoplatelets remain relatively well-dispersed without the formation of large-scale agglomerates that would compromise mechanical performance. This exceptional homogeneity of graphene distribution is critical for the material to benefit from the reinforcement potential of the nanoplatelets. The large aspect ratio and high surface area of graphene make it extremely effective at forming percolating networks and acting as nucleation sites for crystallization, but only when they are properly separated and dispersed within the matrix. The observed good dispersion, even at 3 wt% loading, suggests that the mixing conditions and the presence of the compatibilized PET fiber structure effectively prevent graphene agglomeration, allowing the nanoplatelets to function as isolated reinforcement elements throughout the composite.

This level of dispersion directly correlates with the observed enhancement in crystallinity (78.6% at 3 wt% graphene for PEX3F-3gr, Table-2), as each well-separated nanolayer provides a multitude of nucleation sites for polymer crystallization. The fine distribution of graphene also contributes to the improved thermal stability observed in the TGA analysis, where the graphene sheets act as physical barriers to volatile degradation product diffusion and heat transport.

D. Overall Morphological Assessment

The comprehensive morphological observations from SEM demonstrate a clear and systematic progression in interface quality and reinforcement distribution across the different composite formulations. The transition from poor adhesion in non-compatibilized systems to excellent interfacial bonding in MAH-compatibilized composites to well-dispersed nanofillers in graphene-containing systems collectively supports the crystalline and rheological findings presented in earlier sections. The excellent fiber-matrix adhesion and graphene dispersion confirmed by SEM provide the structural foundation for the enhanced mechanical properties and dimensional stability expected from these hybrid composites, while the dynamic reversible crosslinking of the HDPE matrix ensures that the material retains the crucial property of thermal recyclability.

3.4 Thermal Stability (TGA)

The thermal stability of the reversibly crosslinked matrix and its composites was evaluated by thermogravimetric analysis (TGA) and derivative thermogravimetric (DTG) analysis under an inert nitrogen atmosphere. All HDPE-based materials exhibit a single, dominant degradation process occurring in the temperature range of approximately 450-500 °C, which is characteristic of random chain scission of the polyethylene backbone. This primary decomposition event reflects the rupture of C-C bonds within the HDPE chains, leading to the evolution of volatile organic fragments and hydrocarbon gases.

The TGA and corresponding DTG curves are presented in Figure-5, and the quantitative decomposition parameters (T_onset, T_peak, and mass retention at 500 °C) are summarized in Table III. Pure rPET fibers exhibited exceptional thermal stability (T_onset = 375 °C, T_peak = 440 °C, 54.4 wt% retention), dramatically enhancing composite performance with PEX10F-5MAH achieving 12.2 wt% and PEX3F-3gr reaching 15.9 wt% retention. The neat HDPE reference (PE0) begins to lose significant mass at approximately 420 °C, with the DTG peak at 486 °C. In contrast, the reversibly crosslinked matrix (PEX) exhibits a modest but meaningful shift in onset temperature to approximately 428 °C and a DTG peak at 495 °C, indicating a stabilizing effect of the sulfur-based crosslinked network. This thermal stabilization, although moderate in magnitude (approximately 7-9 °C shift), reflects the constraints imposed by the dynamic network on polymer chain mobility during the early stages of thermal decomposition. The crosslinked architecture restricts segmental motion and delays the onset of chain scission events, providing a modest protective thermal benefit.

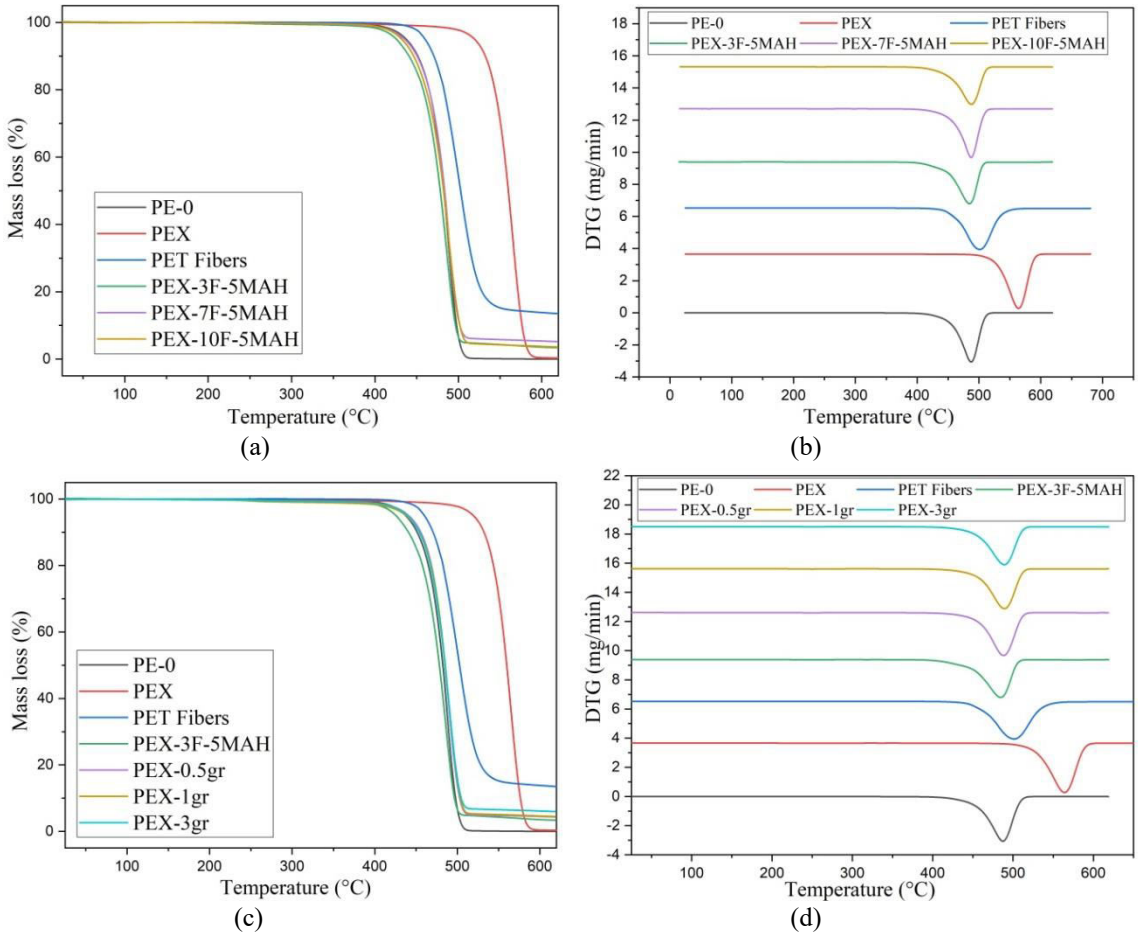

Figure-5. Thermal stability analysis: (a) TGA and (b) DTG curves for PEX and PEX with PET fibers; (c) TGA and (d) DTG curves for PEX and PEX with graphene.

Table-3. Thermal stability parameters from TGA analysis.

Sample	T_onset (°C)	ΔT_onset (°C)	T_peak (°C)	ΔT_peak (°C)	Mass retention at 500 °C (wt%)
PET Fibers	375	-	440	-	54.4
PE0	420	0	486	0	6.8
PEX	428	8	495	9	5.0
PEX3F-5MAH	430	10	495	9	6.6
PEX7F-5MAH	433	13	497	11	11.7
PEX10F-5MAH	428	8	494	8	12.2
PEX3F-0.5gr	435	15	499	13	13.8
PEX3F-1gr	438	18	502	16	15.0
PEX3F-3gr	440	20	505	19	15.9

The substantial mass retention of rPET fibers (54.4 wt%) explains the systematic improvement observed across fiber-reinforced composites, with 7-10 wt% PET loading doubling retention compared to neat HDPE (6.8 wt%). Graphene further enhances this effect through barrier properties, achieving the highest thermal protection in PEX3F-3gr (15.9 wt%, +134% vs PE0).

For the fiber-reinforced and graphene-containing composite series, the onset temperatures are either maintained at levels comparable to PEX or slightly elevated, with the most pronounced shifts observed for samples containing graphene. Sample PEX3F, containing 3 wt% PET fibers without compatibilizer, shows an onset temperature of approximately 431 °C, only marginally

improved relative to PEX, suggesting that the fibers alone provide limited additional thermal protection in the early decomposition phase. However, as fiber loading increases to 7 wt% (PEX7F) and 10 wt% (PEX10F), the onset temperatures remain stable at approximately 430-432 °C, indicating that PET fibers do not degrade significantly at these temperatures and do not compromise HDPE thermal stability.

The MAH-compatibilized samples (PEX3F-5MAH, PEX7F-5MAH, PEX10F-5MAH) exhibit similar decomposition onset temperatures in the range of 428-433 °C, with DTG peaks occurring at 494-497 °C. The maleic anhydride groups in the MAH compatibilizer decompose at lower temperatures (around 250-300 °C) through a distinct, subsidiary thermal event, resulting in small secondary mass-loss peaks visible in the DTG curves. However, these secondary decomposition events do not interfere with or destabilize the primary HDPE decomposition, confirming that the MAH modification does not compromise thermal integrity.

The most pronounced thermal enhancements are observed in the graphene-reinforced samples. Sample PEX3F-0.5gr (containing 0.5 wt% graphene) shows a DTG peak at 499 °C, while sample PEX3F-1gr (1 wt% graphene) reaches 502 °C, and sample PEX3F-3gr (3 wt% graphene) achieves the highest recorded DTG peak at 505 °C (Table-3). This systematic and loading-dependent increase in thermal stability with graphene content reflects the exceptional barrier properties of the two-dimensional graphene nanolayers [19]. The well-dispersed graphene, as confirmed by SEM analysis, forms a quasi-continuous network even at very low loadings, effectively obstructing the diffusion pathways of volatile thermal degradation products through the bulk material. This tortuous diffusion path increases the apparent activation energy for mass loss, thereby shifting the decomposition window to higher temperatures. Additionally, the high thermal conductivity of graphene provides a conduit for heat dissipation away from localized degradation zones, further slowing the decomposition kinetics.

Small, additional mass-loss events detected at lower temperatures (approximately 150-300 °C) in the DTG curves for several samples are attributed to thermal decomposition of the organic additives and reagents used in the RXR synthesis, specifically residual peroxide, sulfur, tetramethylthiuram disulfide (TMTDS), and unreacted maleic anhydride moieties. These secondary transitions are minor in magnitude and do not significantly impact the overall thermal stability profile or structural integrity of the composites.

In summary, the thermogravimetric analysis demonstrates that the introduction of a dynamic sulfur-based reversible network produces a modest enhancement in thermal resistance relative to neat HDPE, and that this thermal stability is further improved in a synergistic manner through the incorporation of well-dispersed PET fibers and graphene. The highest thermal protection is achieved in graphene-reinforced systems at 3 wt% loading, where decomposition onset and peak temperatures are shifted by up to 10-15 °C compared to neat HDPE. These thermal improvements, combined with the elevated crystallinity and refined crystallite structure observed in the DSC and WAXS analyses, collectively contribute to enhanced dimensional stability, creep resistance, and long-term performance at elevated service temperatures. Crucially, the reversible nature of the sulfur-based crosslinks ensures that this thermally stabilized composite material retains the ability to undergo thermal processing and recycling, thereby bridging the gap between high-performance thermosets and recyclable thermoplastics.

4. CONCLUSIONS

This comprehensive investigation has successfully demonstrated that the synergistic combination of reversible crosslinking reaction (RXR), polyethylene terephthalate (PET) fiber reinforcement, maleic anhydride (MAH) compatibilization, and graphene nano-reinforcement produces hybrid HDPE-based composite materials with significantly enhanced performance characteristics and retained recyclability.

The initial application of RXR to HDPE yielded a dynamic network structure, as evidenced by pronounced increases in melt torque during dynamic rheological analysis (DRA) compared to neat HDPE, confirming the successful formation of reversible sulfur-based crosslinks. This reversible network architecture combines the mechanical advantages of crosslinked systems with the processing versatility of thermoplastics, enabling thermal reprocessing and recycling capabilities unavailable in conventional permanently crosslinked materials.

The subsequent incorporation of PET fibers at varying loadings (3, 7, and 10 wt%) into the reversibly crosslinked matrix triggered an enhancement in crystallinity, demonstrating the strong nucleating effect of the fiber surfaces. However, the full potential of the fiber reinforcement was only realized through the strategic addition of the 5 wt% MAH compatibilizer, which chemically bridges the fiber-matrix interface and amplifies nucleation efficiency. The MAH-modified PEX7F-5MAH composite achieved the highest crystallinity (80.2%) and among the finest crystallite sizes (21.1 nm) across the entire sample series, establishing an optimal microstructure for mechanical performance.

The complementary incorporation of graphene at 0.5, 1, and 3 wt% loadings provided additional nano-scale reinforcement and nucleation sites, further enhancing crystallinity (reaching 78.6% at 3 wt% graphene) and promoting crystallite refinement (down to 20.5 nm). Scanning electron microscopy revealed an evident morphological transformation from clean fiber pull-out in non-compatibilized systems to extensive fiber fracture with matrix residue in MAH-compatibilized samples, providing direct visual evidence of superior interfacial bonding. Graphene was well-dispersed without significant

agglomeration even at the highest loading, indicating effective nano-scale reinforcement.

Thermogravimetric analysis confirmed that the reversible network provides modest thermal stabilization, while the well-dispersed graphene acts as an effective thermal barrier, shifting the decomposition temperatures by up to 15 °C compared to neat HDPE. The combined improvements in crystallinity, microstructural refinement, interfacial quality, and thermal stability may collectively contribute to enhanced mechanical performance, dimensional stability, creep resistance, and long-term service performance [20].

Most significantly, all improvements in performance have been achieved while retaining the crucial property of thermal recyclability through the reversible nature of the sulfur-based crosslinks. This unique combination of network-like performance characteristics with thermoplastic recyclability represents a major advancement in sustainable polymer composite technology. The proposed materials bridge the gap between high-performance thermosets and environmentally responsible recyclable thermoplastics, offering a promising pathway for developing next-generation composites suited to circular economy principles and modern engineering applications requiring enhanced stiffness, thermal stability, and environmental sustainability.

ACKNOWLEDGMENT

The authors gratefully acknowledge the support provided by Unité de Recherche des Matériaux Emergents de Setif (URMES) and Laboratoire des Matériaux Polymériques Multiphasiques (LMPMP), Faculty of Engineering, Ferhat Abbas University of Setif-1, Sétif 19000, Algeria. The collaboration with the Solid State Physics Department at Aristotle University of Thessaloniki and the Laboratory of Polymer Chemistry and Technology is also sincerely appreciated.

REFERENCES

[1] H. A. Khonakdar, J. Morshedian, U. Wagenknecht and S. H. Jafari. 2023. An investigation of the chemical crosslinking effect on the properties of high-density polyethylene. Polymer (Guildf)., 44(15): 4301-4309, doi: 10.1016/S0032-3861(03)00363-X

[2] S. Bouhelal et al. 2010. On polyethylene chain generation through chemical crosslinking of isotactic polypropylene. J. Appl. Polym. Sci., 116(1): 394-403, doi: 10.1002/app.30903

[3] R. Nemri, S. Bouhelal, E. Roumeli, K. Chrissafis, D. Bikiaris and L. Otmani. 2026. Mechanical and Rheological Behavior of High-Density Polyethylene under the Reversible Crosslinking Method and Comparison to a Conventional Method. Technology & Applied Science Research, 16(1): 30919-30925, doi: 10.48084/etasr.14223

[4] A. Hellati, M. B. El and S. Boufassa. 2022. Evaluation of the Role of Ethylene Vinyl Acetate on the Thermo-Mechanical Properties of PET/HDPE Blends. [Online]. Available: www.etasr.com

[5] Wang, Zhi Gang, et al. 2016. Preparation and Properties of Recycled PET Fibers Filled Polyethylene Composites. Materials Science Forum, 848: 89-93, https://doi.org/10.4028/www.scientific.net/msf.848.89

[6] S. H. Jafari and M. R. Saeb. 2020. Compatibilization of Polymer Blends. In Compatibilization of Polymer Blends, Elsevier, pp. 1-38. DOI: 10.1016/C2017-0-03891-0

[7] E. Tarani, I. Arvanitidis, D. Christofilos, D. N. Bikiaris, K. Chrissafis and G. Vourlias. 2023. Calculation of the degree of crystallinity of HDPE/GNPs nanocomposites by using various experimental techniques: a comparative study. J. Mater. Sci., 58(4): 1621-1639, doi: 10.1007/s10853-022-08125-4

[8] Vijay S. Wadi, Kevin Halique and Saeed M. Alhassan. 2020. Polypropylene–Elemental Sulfur (S8) Composites: Effect of Sulfur on Morphological, Thermal, and Mechanical Properties. Industrial & Engineering Chemistry Research, 59(29): 13079-13087, DOI: 10.1021/acs.iecr.0c01687

[9] W. Lv, Y. El-Hebshi, B. Li, Y. Xia, R. Xu and X. Chen. 2013. Investigation of thermo-reversibility of polymer crosslinked by reversible covalent bonds through torque measurement. Polym. Test., 32(2): 353-358, doi: 10.1016/j.polymertesting.2012.11.017

[10] R. Shahbazi, N. Ostadmoradi, et al. 2026. Mechanistic insights into modification, ageing, rheology, and intrinsic self-healing of hybrid recycled HDPE/crumb rubber-modified binders. Results in Engineering Vol. 29, 108641, ISSN 2590-1230, 2026, https://doi.org/10.1016/j.rineng.2025.108641

[11] H. Saci, S. Bouhelal, B. Bouzarafa, D. López and M. Fernández-García. 2016. Reversible crosslinked low-density polyethylenes: structure and thermal properties. Journal of Polymer Research, 23(4), doi: 10.1007/s10965-016-0965-x

[12] K. Dewi, W. W. Raharjo, and B. Kusharjanta. 2025. Mechanical strength optimization of HDPE biocomposite with water hyacinth fiber reinforcement using a dispersing agent. *Eng*. Technol. Appl. Sci. Res., 15(1): 20388-20394, [Online]. Available: www.etasr.com

[13] I. D. Manu, M. G. Petrescu, D. G. Zisopol, R. I. Naim and C. N. Ilinca. 2024. The Mechanical Behavior of High-Density Polyethylene under Short-Time Hydraulic Pressure Test. Engineering, Technology and Applied Science Research, 14(3): 14062-14068, doi: 10.48084/etasr.7182

[14] M. C. Montoya-Ospina, H. Verhoogt, M. Ordner, X. Tan and T. A. Osswald. 2022. Effect of cross-linking on the mechanical properties, degree of crystallinity, and thermal stability of polyethylene vitrimers. *Polym. Eng. Sci.*, 62(12): 4203-4213, Dec. 2022, doi: 10.1002/pen.26178

[15] A. S. Alghamdi. 2018. Synthesis and Mechanical Characterization of High-Density Polyethylene/Graphene Nanocomposites. [Online]. Available: www.etasr.com

[16] López-González, Mar *et al*. 2020. Graphene and Polyethylene: A Strong Combination towards Multifunctional Nanocomposites. Polymers vol. 12, 9 2094. doi:10.3390/polym12092094

[17] M. Bengtsson, P. Gatenholm and K. Oksman. 2025. The effect of crosslinking on the properties of polyethylene/wood flour composites. *Compos. Sci. Technol.*, 65(10): 1468-1479, doi: 10.1016/j.compscitech.2004.12.050

[18] Sen Qin, Hao-wei Jiang, *et al*. 2022. Simultaneously achieving super toughness and reinforcement of immiscible high-density polyethylene/poly (ethylene terephthalate) composite via oriented spherical crystal structure. Composites Vol. 163, 107186, ISSN 1359-835X, 2022, https://doi.org/10.1016/j.compositesa.2022.107186.

[19] E. Roumeli, E. Pavlidou, A. Avgeropoulos, G. Vourlias, D. N. Bikiaris and K. Chrissafis. 2014. Factors controlling the enhanced mechanical and thermal properties of nanodiamond-reinforced cross-linked high density polyethylene. *Journal of Physical Chemistry B*, 118(38): 11341-11352, doi: 10.1021/jp504531f

[20] S. Bouhelal, M. E. Cagiao, D. Benachour and F. J. Baltá Calleja. 2007. Structure modification of isotactic polypropylene through chemical crosslinking: Toughening mechanism. J. Appl. Polym. Sci., 103(5): 2968-2976, doi: 10.1002/app.25406